

## The anti-lotus leaf effect in nanohydrodynamic bump arrays

This article has been downloaded from IOPscience. Please scroll down to see the full text article.

2010 New J. Phys. 12 085008

(<http://iopscience.iop.org/1367-2630/12/8/085008>)

View [the table of contents for this issue](#), or go to the [journal homepage](#) for more

Download details:

IP Address: 128.112.48.116

The article was downloaded on 16/02/2011 at 15:16

Please note that [terms and conditions apply](#).

## The anti-lotus leaf effect in nanohydrodynamic bump arrays

Keith Morton<sup>1</sup>, Ophelia K C Tsui<sup>2</sup>, Chih-Kuan Tung<sup>3</sup>,  
James C Sturm<sup>4</sup>, Stephen Y Chou<sup>4</sup> and Robert Austin<sup>5,6,7</sup>

<sup>1</sup> National Research Council, Montreal, QC, Canada

<sup>2</sup> Department of Physics, Boston University, Boston, MA, USA

<sup>3</sup> Department of Physics, Hong Kong University of Science and Technology, Kowloon, Hong Kong

<sup>4</sup> Department of Electrical Engineering, Princeton University, Princeton, NJ, USA

<sup>5</sup> Department of Physics, Princeton University, Princeton, NJ, USA

<sup>6</sup> Visiting Member, Institute for Advanced Study, Hong Kong University of Science and Technology, Kowloon, Hong Kong

E-mail: [austin@princeton.edu](mailto:austin@princeton.edu)

*New Journal of Physics* **12** (2010) 085008 (14pp)

Received 1 September 2009

Published 19 August 2010

Online at <http://www.njp.org/>

doi:10.1088/1367-2630/12/8/085008

**Abstract.** In this paper, we address the hydraulic flow of fluids on and within nanofabricated hydrophilic (as opposed to hydrophobic) surfaces, and the influence of an extended precursor film on the wetting dynamics of water penetrating a nano-textured array of posts that has no sealing surface (open-top). The width of the precursor film in front of the wetting edge  $\delta$  is extraordinarily large, approximately 2 mm for our device, and it drives the wetting penetration film in the open-top array. We discuss the way this thin precursor film controls the movement of the macroscopic wetting front  $L_w$  and its dynamics in the nanofabricated array of posts. Rapid and controllable transport of nanoparticles in such an open top array of posts, as controlled by the precursor film, is demonstrated using a bump array textured morphology.

<sup>7</sup> Author to whom any correspondence should be addressed.

**Contents**

<b>1. Introduction</b>	<b>2</b>
<b>2. Basic theory</b>	<b>2</b>
<b>3. Methods and materials</b>	<b>7</b>
<b>4. Results</b>	<b>9</b>
<b>5. Conclusions</b>	<b>13</b>
<b>Acknowledgments</b>	<b>13</b>
<b>References</b>	<b>14</b>

**1. Introduction**

The present paper explores the effect of nanofabricated surfaces on the wetting dynamics of fluids on hydrophilic surfaces, and how nanoflow caused by wetting dynamics can effectively transport objects in nanoarrays. The nanoarray we use here is a highly ordered array consisting of a rotated square lattice of posts; the rotation of the array relative to the average flow direction gives rise to the unusual transport properties of colloidal particles in the array [1]. Unfortunately, in such a short paper as this we can do justice to neither the complexity of the dynamics of colloidal particles in a rotated nanoarray (a nanobump array) nor the complexity of how water, a volatile and highly polar fluid, wets such an array. We hope we can point out some fascinating aspects of the dynamics of these two problems.

The emphasis of this paper is really on the transport of objects in an open-top nanobump array, not the wetting physics *per se*. However, there is a problem with nanobump arrays that forces us to consider the wetting dynamics. The problem is that as the dimensions of arrays used for sorting particles shrink to the nanoscale, the hydrodynamic impedance of the device, defined as the pressure/length gradient needed for a given flux of fluid flow, becomes prohibitively high. One potential way around this problem is to run the device ‘open-top’, that is, without a top sealing the device, and let evaporative transport generate the flux drive. Opening the top decreases the shear gradients, and use of evaporation removes the need for high-pressure external pumps, in principle. This experimental paper shows that this scheme has the potential to work.

Ordinarily, we would show the results first and then present the theory to explain the results. However, we felt in this paper that it would perhaps be best to first outline the theory and then show how the theory might begin to explain the results. Unfortunately, we are dealing with an extremely complex system: out of equilibrium flow of a volatile liquid in a nanostructured open-top device where significant evaporation is occurring. We can only sketch out a few lines of analysis that illuminate basic, hopefully relevant, aspects of the complexity of the problem. The good news is that, despite the complexity, in fact it is possible to have high rates of flow in such an open-top nanostructured nanobump array and achieve high-resolution fractionation in the open-top evaporative drive configuration.

**2. Basic theory**

There has been a great deal of discussion recently about the influence of nanostructuring of *hydrophobic* surfaces on the *decrease* of the wetting properties of water to the point of total

exclusion of the liquid from the surface. This total exclusion of water by a nano-textured hydrophobic surface is called the lotus-leaf effect, in analogy to the remarkable non-wetting and self-cleaning properties of the lotus leaf [2]. Hydrophilic nanostructured surfaces, as opposed to hydrophobic nanostructured surfaces, are perhaps more interesting dynamically because they do wet the surface. In particular, as we stated in the introduction, we are interested in decreasing the hydrodynamic resistance using nanostructures, and exploiting evaporation of volatile fluids to drive flow functionally through nanostructured surfaces.

The shear gradients are driven by boundary conditions and drive the pressure gradients. One of the fundamental assumptions in macroscopic hydrodynamics is the presence of a stick-boundary surface where fluid voxels are at rest with respect to the surface [3]. The argument for the apparent necessity of a stick-boundary surface is very simple. In a fluid of viscosity  $\eta$ , the local shearing stress  $\sigma_{xz} = F_x/A_{xy}$  in the  $\vec{x}$ -direction is proportional to the local transverse shear in the  $\vec{z}$ -direction normal to the surface:

$$\sigma_{xz} = \frac{F_x}{A_{xy}} = \eta \frac{\partial v_x}{\partial z}. \quad (1)$$

Hence, if the local stress is to be finite the gradients in velocity must be finite and there cannot be fluid at the wall surface moving with a finite velocity parallel to the wall, giving rise to an infinite shear. The perceived necessity for fluid voxels in contact with the wall to be at rest relative to the wall gives rise to stick boundary conditions, which circumvents the divergence problem for slip at the boundary.

It is less well known that equation (1) is not the only possible boundary condition that satisfies the Navier–Stokes equation [4, 5]. In freshman physics, we routinely handle frictional forces by assuming that a solid moves with finite slip speed  $v_s$  relative to another surface giving rise to a drag force proportional to a coefficient of friction  $\kappa$ . A similar model might apply for fluids moving near a wall. We assume a linear relation between the drag force and the slip velocity of the surface moving through the fluid:

$$\sigma_{xz} = \kappa v_s, \quad (2)$$

where  $\kappa$  is the drag coefficient. We then can assume that at the wall ( $z = 0$ ):

$$v_s = \frac{\eta}{\kappa} \frac{\partial v_x}{\partial z} = b \frac{\partial v_x}{\partial z}, \quad (3)$$

where  $b$  is defined as the slip length. In this model, there is finite slip at the surface. It has been proposed [6] that this slip-boundary condition can profoundly change the hydrodynamic impedance of nanopatterned surfaces.

A related issue to the possible failure of stick-boundary conditions is the dynamics of wetting of surfaces by liquids, and the effect of nanopatterning of a surface on the wetting profile. In the case of a smooth surface, a liquid drop that partially wets a solid surface will form a contact angle  $\theta_C$  between the surface of the liquid and the solid surface. See figure 1 for the definition of the contact angle  $\theta_C$ . The surface wetting phenomenon involves three states of matter and their interaction, as expressed by surface tensions between the states: the gas phase  $G$  of the wetting fluid, the liquid phase  $L$  of the wetting fluid and the solid state that is being wet  $S$ . If  $\gamma_{GL}$  denotes the surface tension between the gas and the liquid,  $\gamma_{SG}$  the surface tension between the solid and the gas and  $\gamma_{SL}$  the surface tension between the solid and the liquid, then the Young relation [11] gives

$$\gamma_{SG} - \gamma_{SL} = \gamma_{LG} \cos \theta_C = A_{ad}, \quad (4)$$

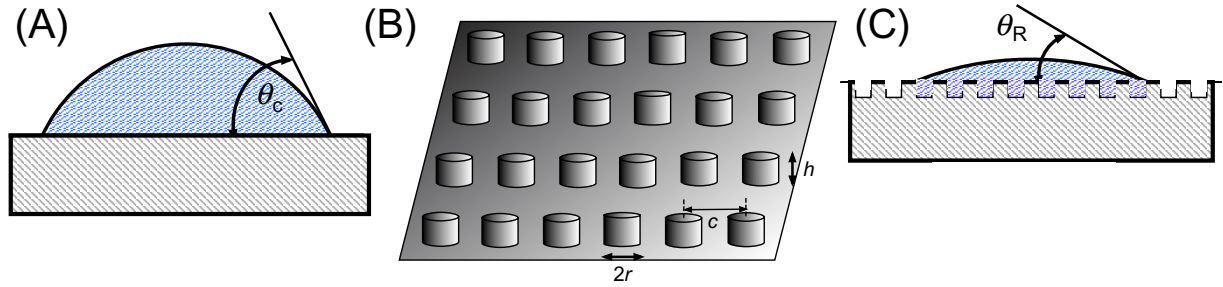


**Figure 1.** Classical Wenzel wetting concepts. (A) The contact angle  $\theta_C$  for a smooth surface. (B) A textured surface consisting of cylinders of height  $h$  and radius  $r$  separated by center-to-center distance  $c$ . (C) Modification of the contact angle to  $\theta_R$  due to the roughness of the underlying substrate surface.

where  $A_{\text{ad}}$  is called the adhesion (in units of force/length) of the liquid to the solid [9]. For water at 25 °C,  $\gamma_{LG} = 70 \text{ dynes cm}^{-1}$ , and for water on quartz  $\theta_C$  is 30°, thus  $\gamma_{SG} - \gamma_{SL} = A_{\text{ad}}$  is 61  $\text{dynes cm}^{-1}$  [7].

In spite of the positive number of  $A_{\text{ad}}$  for water on quartz, this does not mean that water will wet quartz, since  $\theta_C = 30^\circ$ . Spreading of a fluid on a surface that wets it (i.e. a hydrophilic surface) must result in the release of free energy. A critical parameter in spreading dynamics is the spreading parameter  $S$ , which sets the sign of  $\cos \theta_C$ :

$$S = \gamma_{SG} - \gamma_{SL} - \gamma_{LG} = A_{\text{ad}} - \gamma_{LG}. \quad (5)$$

Note that  $S$  is a measure of the interfacial free energy gained by a spreading drop. If  $S > 0$  complete wetting of a surface will happen and  $\theta_C = 0$ , whereas if  $S < 0$  the drop will form an equilibrium shape on the surface and not wet it, with a distinct wetting line  $L_w$ . Water will not wet a smooth clean quartz surface because  $S < 0$ , namely  $-9 \text{ dynes cm}^{-1}$ . We will see later that water, however, does wet a nanotextured quartz surface.

The movement of the wetting line  $L_w$  on a wetting surface is complex. The wetting dynamics in our case have no significant inertial terms. The capillary number  $C_p$  is related to the Reynold number  $Re$  of hydrodynamics and sets the contribution of the inertial terms in the flow at speed  $v$ . The more familiar  $Re$  is defined as the ratio of the inertial terms in the Navier–Stokes equation to the viscous damping times in a flow:

$$Re = \frac{\rho v L}{\eta}, \quad (6)$$

where  $\rho$  is the mass density of the flow and  $L$  is some characteristic length scale over which the voxels change their direction. Flows at low  $Re$  have the viscous term dominate and the flow is overdamped. A delightful introduction to  $Re$  can be found in the classic article by Purcell [8]. In our case,  $Re$  is of the order of  $10^{-4}$  assuming that  $v \sim 100 \mu\text{m s}^{-1}$  and  $L \sim 100 \text{ nm}$ , so we are completely in the low  $Re$  regime. The capillary number  $C_e$  is a measure of the ratio of the viscous force terms to the surface tension forces in a wetting front moving at speed  $v$ :

$$C_e = \frac{\eta v}{\gamma_{LG}}. \quad (7)$$

In our case for water  $C_e \sim 10^{-6}$  and so surface tension terms dominate the flow.

Further, the prediction is that the spreading rate (the speed  $v$  at which the wetting line  $L_w$  moves across the surface) of a drop for  $S > 0$  should scale with  $S$ : a larger  $S$  should result in a fast speed  $v$  of the macroscopic wetting front,  $v = dL_w/dt$ . In this view, the wetting line  $L_w$  moves as a distinct line over a dry surface, wetting it. For volatile liquids such as water, the liquid evaporating from the drop can condense as a thin film in front of the drop interface and the drop will wet by moving over a thin film of condensed phase called the precursor film, hence locking  $S$  at zero and removing any  $S$  dependence on the wetting rate.

However, the precursor film can also occur for both volatile and non-volatile fluids [12], as deGennes has discussed [9]. In fact, there is a hydrodynamic reason why there must be a precursor film in a wetting process: the viscous dissipation due to shear in a film of thickness  $x$  scales as  $1/x$  and so a contact line moving across a dry surface will have a diverging shear force without the existence of a precursor film, which acts as a slip boundary layer [9]. One can view this as another way to obtain slip boundary conditions, by movement of the macroscopic wetting front  $L_w$  over the thin precursor film. Furthermore, since, as deGennes pointed out, virtually all of the viscous dissipation in the fluid occurs where the shear is highest, we can guess that it is the dissipation in the precursor film that drives the primary wetting dynamics.

Roughening or texturing the surface changes both the statics and dynamics of wetting. If the surface is not smooth but textured, the Young relation given by equation (4) does not apply. The contact angles  $\theta_C$  for a textured but chemically homogeneous surface can be greatly different from that predicted by equation (4). Wetting of a textured surface can be quite a complicated process, but there is an empirical relation called Wenzel's equation, which can be used to estimate the actual contact angle for a rough surface  $\theta_R$ , given the smooth surface contact angle  $\theta_C$  [13]:

$$\cos \theta_R = R \cos \theta_C, \quad (8)$$

where  $R$  is the surface roughness ratio of the total surface area of the rough surface  $A_R$  to the smooth surface  $A_s$  and is thus always  $>1$ . Since a neutral surface has  $\theta_C = \pi/2$  and hence  $\cos \theta_C = 0$ , the effect of roughness is to decrease the angle for a hydrophilic surface ( $\theta_C < \pi/2$ ) and increase the angle for a hydrophobic surface ( $\theta_C > \pi/2$ ). Complete wetting will occur for surfaces with roughness such that  $\cos \theta_R > +1$  and complete repulsion occurs if the surface has  $\cos \theta_R < -1$ . We are concerned with the super-hydrophilic surfaces in this paper, which we call the anti-lotus leaf effect.

Although we have an unusual pattern for the posts, a bump array [1], basically our textured surface has an increased area  $\Delta A$  due to the sides of the posts. If the center-to-center post-post spacing is  $c$  and the posts are of radius  $r$  and height  $h$ , the roughness  $R$  of our surface is

$$R \sim 1 + \frac{2\pi r h}{c^2}. \quad (9)$$

Figure 1 shows the definition of the various parameters used in these equations.

It was previously shown by McHale *et al* [14] that the simple Wenzel relationship equation (8) could be used to model the *static* macroscopic wetting of a liquid in an array of posts made of a hydrophilic material and the evaluation of the macroscopic contact angle. Ishino and Okumura [15] have shown that the effect of texturing the surface does more than simply change the contact angle as described by equation (8). If the material is hydrophilic, the precursor film forms a thin penetration film that enters into the structured surface in advance of the wetting edge  $L_p$  and has an edge  $L_p$ , with width  $\delta$ . In the words of Ishino and Okumura, the drop looks like a sunny-side-up egg sitting on the surface, with the yolk as the center of

the drop and the precursor film as the thin egg white surrounding the yolk. This precursor film with edge line  $L_p$  does not have a constant thickness, but roughly the average thickness  $h$  is [9]

$$h \sim a \times \sqrt{\frac{3\gamma_{LG}}{2S}}, \quad (10)$$

where  $a$  is the range of the van der Waals force (of the order of 0.1 nm). For water on the nano-textured quartz surfaces, discussed later, where the spreading parameter  $S$  is positive, we expect that  $h \sim 10$  nm, but this is dependent on the unknown wetting parameter  $S$  for a nano-textured surface.

The width  $\delta$  of the precursor film is a function of the speed of the wetting front and hence a dynamic quantity. A discussion of the dynamics of the precursor wetting film dynamics can be found in the paper by Bonn *et al* [10]. Briefly, the greater the rate at which the precursor film is pulling the fluid across the surface, the shorter the width  $\delta$ . de Gennes [9] showed that

$$\delta \sim a \times \sqrt{\frac{S}{\gamma_{LG}}} \times \frac{1}{C_e} = a \times \sqrt{\frac{S}{\gamma_{LG}}} \times \frac{\gamma_{LG}}{\eta v}, \quad (11)$$

where we have explicitly written the expression for  $C_e$ .

Nanoscale roughness of a surface could increase  $\delta$  because of the locally increased surface area of the nanoscale rough surface. We can use Wenzel's conjecture equation (8) and further conjecture that the width of the precursor film in a rough medium  $\delta$  for a surface of roughness  $R$  is increased by the factor

$$\delta^R \sim \frac{\delta}{\cos^{-1}(R \cos \theta_C)}. \quad (12)$$

Note that we are extrapolating from static analysis to the much less known dynamic system, so equation (12) is not to be taken very firmly. Clearly, it is possible, then, for  $\delta$  to become very large as  $\cos^{-1}(R \cos \theta_C)$  approaches 0 for sufficiently large values of  $R$ . This effect of enhanced penetration of the precursor film in a rough matrix is a dynamic 'anti-lotus leaf effect', since Wenzel's conjecture was proposed for a drop at equilibrium, whereas equation (12) applies to the situation where the drop is spreading. Even the presence of a precursor film is rather unexpected in a nanoarray made of a hydrophilic material, in that we would guess that the capillary forces exerted by the posts on the fluid would draw the precursor film to line the side wall of the posts and thus lift the fluid rapidly to the surface, creating only a macroscopic wetting line  $L_w$ .

Modeling the time dependence of the wetting flow in the nanoarray is of course a very complex issue. Very naively, we can expect that the driving force  $F_{\text{drive}}$  acting on the fluid moving in the gap between posts of gap width  $(c - 2r)$  should roughly scale as  $\gamma_{LG} \times (c - 2r)$ . This yields the Washburn equation for the rate at which the liquid can penetrate the array:

$$z(t) \sim \left[ \frac{2\gamma_{LG}(c - 2r)}{\eta} t \right]^{1/2}, \quad (13)$$

where  $\left[ \frac{2\gamma_{LG}(c - 2r)}{\eta} \right]$  acts like an effective dynamic diffusion coefficient  $D_d$ . Note that  $D_d$  scales as the square root of the gap spacing  $(c - 2r)$ , indicating that nanoarrays should wet more slowly than microarrays. However, there is still an enormous enhancement for millimeter-size drops spreading on a textured surface as opposed to a smooth surface, as noted by Ishino *et al* [16], since a drop on a smooth surface only has gravitational forces driving the wetting, whereas

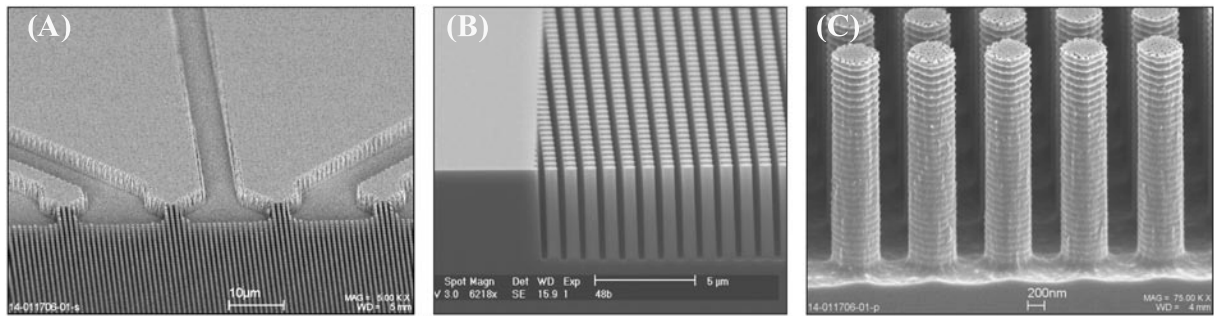


**Figure 2.** (A) The photolithographically constructed feeder channels to the nanofabricated bump array. (B) The phase-shifted bump array constructed using NIL. (C) Detail of the posts in the array.

a drop on a textured surface has the capillary forces adding to the driving forces, yielding enhancement in spreading rates of the order of  $10^5$ .

### 3. Methods and materials

A combination of standard photolithographic techniques and nano-imprint lithography (NIL) [19] techniques were used to create an array of posts with submicron inter-post spacing  $c$ , defined above [20, 21]. In order to test the effectiveness of open-top transport using the pulling action of the precursor film, as the nanotextured structure we choose a ‘bump-array’ format, which is a phase-shifted microfluidic array [1] that separates particles deterministically. One of the challenges of this technology is scaling to the nanoscale where the hydrodynamic impedance becomes extremely high; we wished to test the use of an open-top nanoflow system and the pulling on the precursor film as an efficient way to obtain high flow rates. In NIL, an imprint mold is used to pattern a thin, curable polymer layer on a substrate. Due to the high fidelity of the imprint process, features are replicated precisely and mold quality is critical to high-resolution nanoimprinting. The pillar molds were fabricated using a daughter mold fabrication process where two cycles of NIL (including subsequent pattern transfer by standard reactive ion etching) are carried out with a one-dimensional (1D) grating mold. In the second cycle, the 1D grating mold was rotated to the desired angle for the bump array to create a 2D array of pillars.

The original 1D grating mold was patterned on 4 in diameter wafers by interference lithography. UV interference lithography with a 351 nm Ar-ion laser source (SabreUV, Coherent) was used to make the initial 1D grating features in an i-line photoresist (AZ7905, AZ electronic materials), part of a tri-layer resist stack that also included a 15 nm layer of evaporated  $\text{SiO}_2$  on top of a 180 nm thick UV absorbing ARC layer (xHiRC, Brewer Science). Following exposure and development, the 1D grating patterns were transferred through the resist stack and into the substrate and used to pattern the 2D pillar molds. These low aspect ratio (1:1), 2D pillar molds were used as masters to prepattern the silicon substrates for reactive ion etching. Details of this procedure can be found in [21]. Figure 2 shows a scanning electron microscope image of the nanofabricated bump array.

Our nano-post arrays are a special design with a phase shift between rows. The nano-post array shown in figure 2 is one of the most aggressive designs, with the minimum gap spacing possible using optical techniques. The post array has a phase shift  $\epsilon$  of 0.1, a center-center

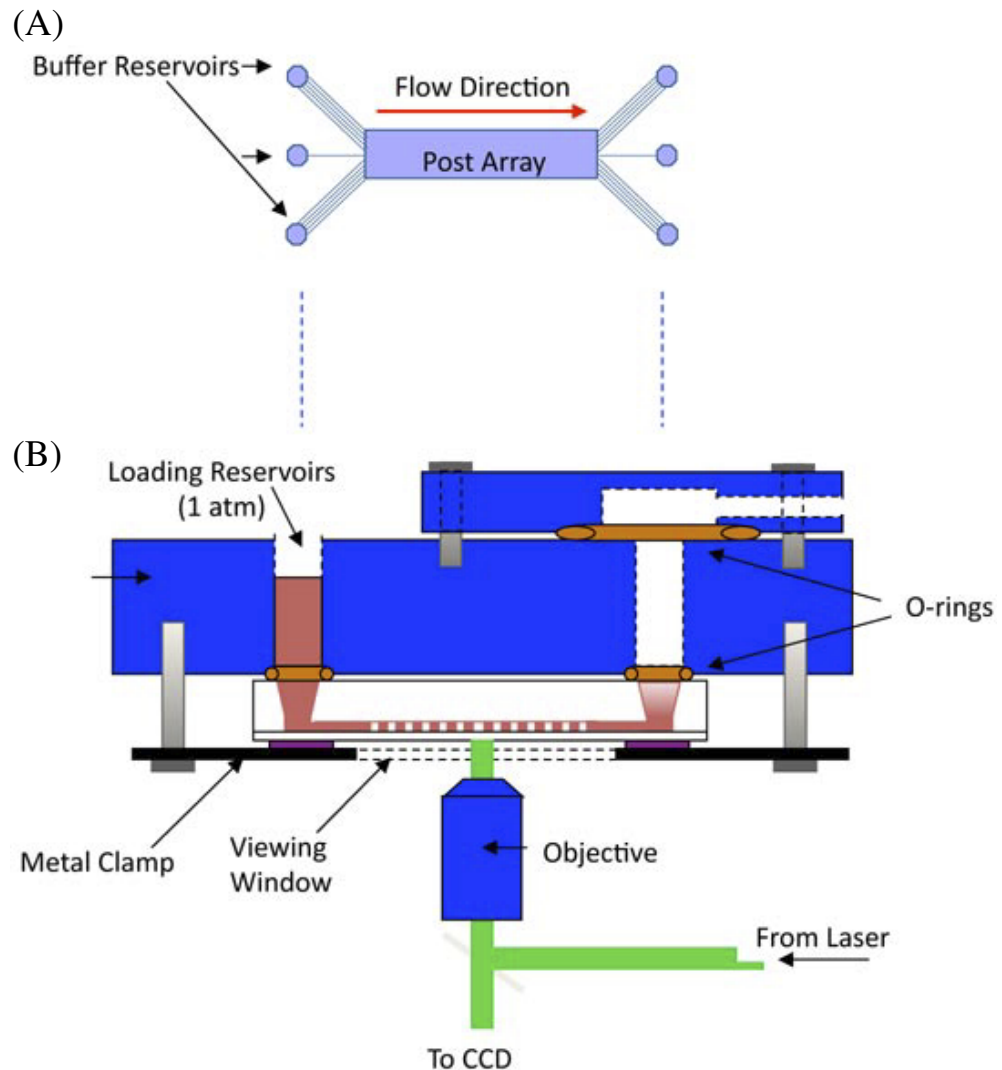


**Figure 3.** (A) The basic flow pattern of fluids in the array. (B) Schematic of the chip jig in which the optical measurements were made.

spacing  $c$  of 1000 nm and a 400 nm gap between the posts; the posts have a radius  $r$  of 200 nm, and a post height  $h$  of 2800 nm. This array has a very high roughness  $R$  of 1.45. Since  $\theta_C$  for water on quartz is  $30^\circ$ , the use of Wenzel's equation (8) yields an unphysical value for  $\theta_R$  and hence the array should be super-hydrophilic.

The nanostructured chips were sealed using a polydimethylsiloxane (PDMS)-coated coverslip over only a fraction of the nanofabricated area ranging from 10% to 90% of the nanostructured area. The chip was held in a custom jig, which allowed simultaneous epifluorescence measurements of particle motion in the chip (or bright-field imaging), and blowing of compressed air streams over the unsealed region of the chip. Figure 3 shows the basic design of the experiments.

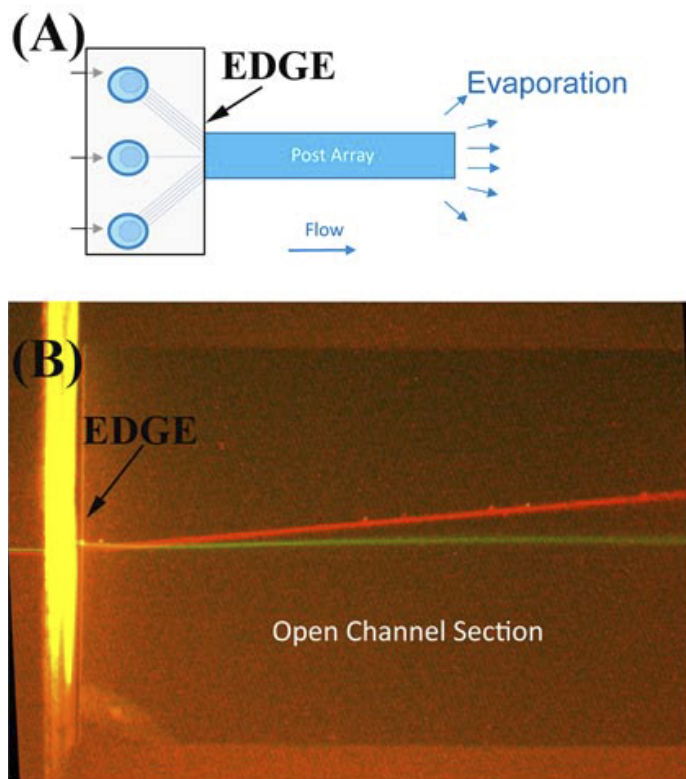


**Figure 4.** (A) Schematic of a partially sealed array. (B) Epifluorescence image of red beads ‘bumping’ at an angle to the flow direction given by the green dye jet. The flow across the device is driven by evaporation.

Figure 4 shows how the chip was partially sealed with a sealed inlet region and an ‘open top’ observation region. Compressed air was passed over the open region and the evaporation of the water drove fluids through the nanopatterned bump array. 300 nm diameter red fluorescent beads were loaded into the center feed port of the device, along with a solution of green fluorescent dye to make the center channel flow streams. Figure 4 shows that under steady state air flow, the beads in the open-top area were transported across the array and the bump nanoarray was able to successfully operate as a fractionating device without clogging due to the steady transport of water from the sealed area. Estimated particle flow velocities of thousands of microns per second could be easily achieved by simply modulating the air steam flow, while the input port pressure head remained at atmospheric pressure.

#### 4. Results

When water with a 5 mm pressure head enters the nanoarray via the feeder tubes, there is a rapid wetting of the nanochannel array in about 5 s for several centimeters, hence the expected great acceleration of the wetting process compared to a smooth surface predicted by equation (13) and [16] is evident. We also observed using white epi-illumination two distinct fronts: a macroscopic wetting front  $L_w$  and a thin precursor front  $L_p$ , separated by a distance  $x_{\min}$ , which we tentatively identify with the width  $\delta$  of the precursor film discussed in the theory section, but will label as  $x_{\min}$  in the following figures.

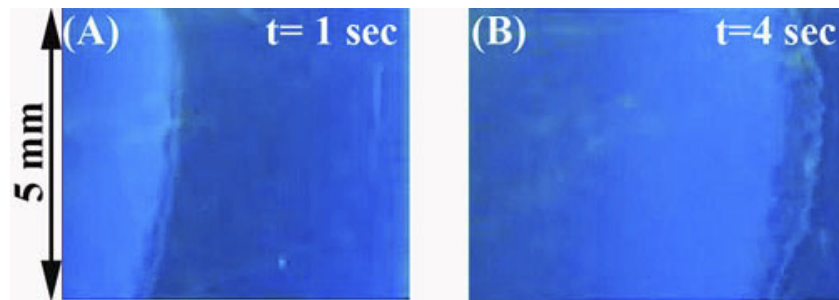


**Figure 5.** (A) Wetting front into a bump array at  $t = 1$  s after wetting from the left side. (B) The same front at  $t = 4$  s. The precursor film barely visible in (A) has now grown substantially in size.

Figure 5 shows in epi-illumination the wetting of the array at two different times during the initial wetting process. Note that the precursor film  $L_p$  seen here probably should not be confused with the wetting film fronts  $L_w$  seen in wetting experiments in microfabricated arrays by Courbin *et al* [18] or Ishino *et al* [16]. Our claim is that in front of this main wetting front is a much thinner one, which corresponds to the expected high-shear front that allows wetting to proceed. Courbin *et al* [18] sketch out such a front precursor front, but did not observe it, possibly because their post spacing of  $100\ \mu\text{m}$  is of the order of 200 times greater than our nanoposts, with  $400\ \text{nm}$  gaps, and of the order of the precursor film size at high wetting speeds, as discussed below.

These two fronts are distinguishable owing to interference effects. When the film wets silicon substrate the index of refraction of the wetting film changes the reflectivity of the silicon. Since water has a greater index of refraction than air, and since silicon has a greater index of refraction than water, for very thin films the interference is positive and one sees a brighter blue reflectance on the wet portion. This initial front is followed by a much more optically distinct wetting front  $L_p$ , which apparently is of a uniform thickness, since it shows no interference color changes from the sharp edge  $L_p$  to the entry channels that feed water into the array. Both the edges  $L_w$  and  $L_p$  present a very rough, fractal-like contour as they move through the array. Figure 6(A) shows in pictorial form what is observed in the microscope: a precursor film proceeds the wetting film by several mm as it moves through the array. At present, we have not carried out detailed measurements of the film thickness using interference optical techniques, but we can make some remarks about what is seen in these preliminary experiments. Figure 6(B) presents a montage of images assembled by video microscopy of a wetting front in the nanoarray at its largest extent when the wetting front has come to a temporary stop.

If we identify the liquid film of width  $x_{\min}$  between the edges  $L_w$  and  $L_p$  as the precursor film of width  $\delta$ , some interesting aspects emerge. First, the film width  $x_{\min}$  starts at a width of  $100\ \mu\text{m}$  and grows to a width of about  $2000\ \mu\text{m}$  when the wetting stalls. Thus, the width does agree qualitatively with equation (11), which predicts that the precursor film width should vary inversely with the film speed  $v$ . However, that calculation was a naive estimate of a very complex structure, and our array represents a much more complex surface than a simple smooth surface. The course of the fronts, both the precursor film and the main wetting film, can be followed in time. Figure 7(A) shows the time course of the penetration of the main front into the nanoarray and the fit to equation (13). It is clear that while the fit is by no means perfect, equation (13)

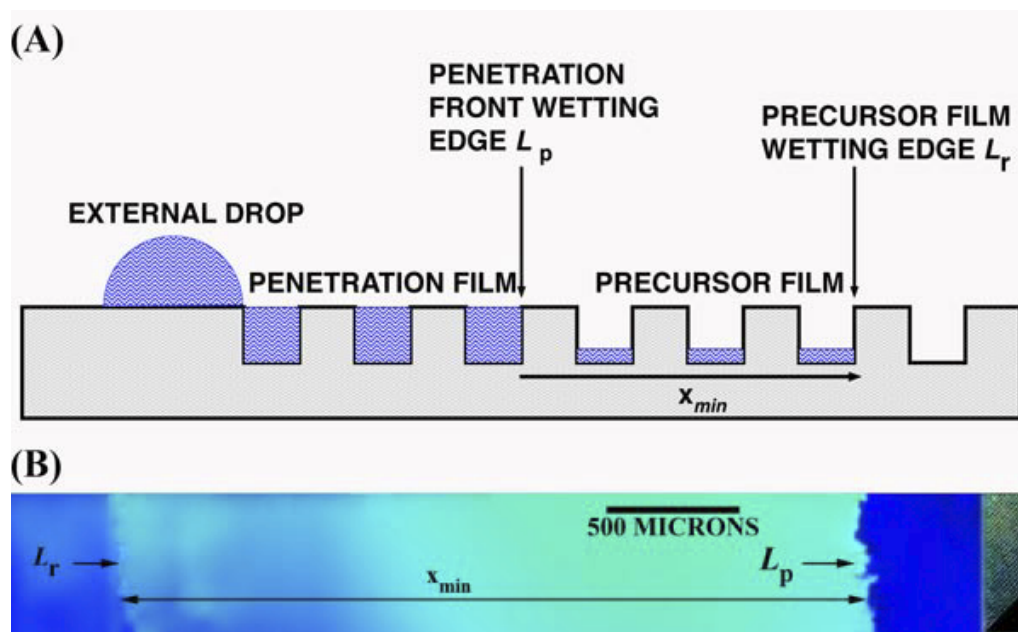


**Figure 6.** (A) Schematic of the observed precursor film in the array. (B) Composite of images of a water front that entered a nanoarray and has come to a stop.

gives a good elementary understanding of the penetration dynamics. The precursor film width has a more complicated and ill-understood dynamic, as seen in figure 7(B). During the initial stages of wetting the precursor film has a time-independent width  $x_{min}$  of approximately 0.2 mm, but as the wetting front slows, the precursor film broadens, becoming over 1 mm wide at 4 s. The macroscopic wetting front  $L_w$  eventually halts due to evaporative losses, and the precursor film becomes over 2 mm wide, as is shown in figure 7.

Further, the precursor film shows clear variations of thickness over the length, which we can only estimate in this preliminary report as being about  $\lambda/4$  of 500 nm visible light, or of the order of 100 nm. There is no one set length for a precursor film even in the absence of evaporation losses, as was shown by Leger *et al* [17]. Leger *et al* observed that the precursor film of PDMS on a smooth surface, while at its thickest value of 60 nm was thinner than our roughly estimated value of 100 nm, also extended out over thousands of microns, so our results are not in great disagreement with one of the few precision measurements. The precursor film is stable and can be controlled by blowing air across the chip surface, controlling the evaporation rate. If no air is blown across the surface, the precursor film moves out across the entire chip, pulling the penetration film with it. If air is blown at a sufficient rate, the precursor film shrinks due to evaporation loss and the penetration film accordingly moves backwards.

This facile movement of the penetration front by controlling the evaporation of the precursor film can be used to move particles in the nanoarray without the use of the high hydrodynamic pressure heads normally needed for movement of fluids through nanostructures. It is possible to estimate the effective pressures that can be exerted by evaporation of fluids in the precursor film by estimating the energy density involved in the latent heat of evaporation  $C_p$  of the fluid, since presumably the free energy burned in the process of transporting the fluid through

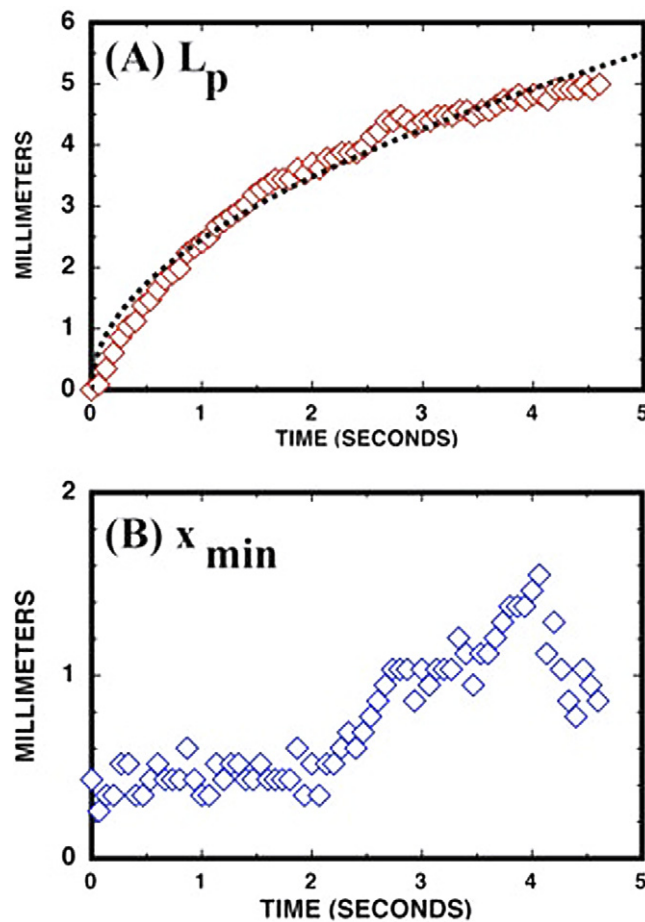


**Figure 7.** (A) Curve fit of equation (13) to the position of the main wetting front  $L_p$  versus time. (B) Time dependence of the precursor film width  $x_{\min}$  versus time.

the array comes from the latent heat of evaporation of the precursor film. For the case of water at 20 °C the latent heat of evaporation per ml of volume  $C_p$  is  $2.4 \text{ J cm}^{-3}$  [7], which corresponds to a pressure of  $2.4 \times 10^9 \text{ N m}^{-2}$ , or  $10^4 \text{ bar}$ , an enormous number due to the huge latent heat of vaporization of water compared to most other liquids. Thus, if water can be evaporated quickly enough via the extreme surface-to-volume ratios that nanofabrication offers, enormous pressure gradients can be created that can rapidly transport nanoparticles through nanostructures with no external pressure heads.

Ordinarily, blowing air or a surface simply dries the water on the surface, leaving behind a residue. There are three major advantages to using a nanopatterned and nanostructured surface: (i) wetting speeds are greatly enhanced using the capillary forces in a structured environment; (ii) water can be brought from an enclosed area into the nanopatterned area continuously feeding fluid into the structure; (iii) by proper design of the nanostructured array particulates can be shunted off to one side and cleared into a waste volume; hence the device is non-clogging. We have been able to demonstrate the potential that open-top nanoarrays have for non-clogging and rapid transport without external pumps with some simple experiments that simply involved blowing air over the end of the nanofilm of water. Figure 8 shows that all the performance

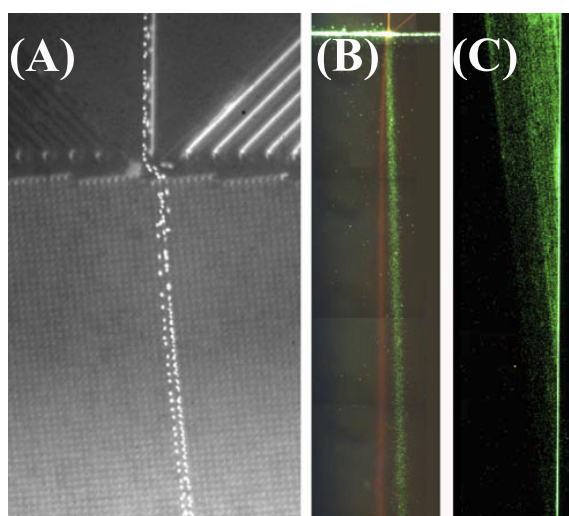


**Figure 8.** Separation of fluorescent spheres in an open-top nanoarray. (A) Precision injection of  $1.6\ \mu\text{m}$  diameter beads in the open-top flow. (B) Separation of  $100\ \text{nm}$  diameter spheres (central diffuse red line) from  $300\ \text{nm}$  spheres in a  $700\ \text{nm}$  pillar spaced open-top nanoarray. (C) Concentration of  $300\ \text{nm}$  diameter beads via the open-top flow. The beads are moving at a rate of several hundreds of microns per second with no external pressure gradient.

features of a sealed ‘bump’ array [1] also work in an open-top device. Although the film is only  $2\ \mu\text{m}$  thick and there is only a  $5\ \text{mm}$  pressure head, liquid is moved rapidly through the array. By very gentle flow of air over the chip, the speed of motion of the liquid can be easily controlled with no external pressure head. In figure 8(C), we show that it is possible to easily move  $300\ \text{nm}$  spheres to the side of a  $700\ \text{nm}$  gap ‘bump’ array at high flow rates of hundreds of microns per second with no external pressure head.

## 5. Conclusions

We have presented preliminary evidence for the presence of a precursor film in front of the space-filling wetting film in an open-top nanofabricated array of posts, which can extend millimeters in front of the wetting front. Application of some basic concepts from the wetting theory of rough surfaces gave a rough agreement for the size-extended precursor film in the open-top array, but the complex dynamics of the film with the wetting front penetration into the array are not understood. The movement of the wetting front in a bump nanopost array facilitates the driving of fluid flow through the array at high speeds without the application of external pressure heads using evaporation alone, and the prediction is that extremely high speeds of  $\text{mm s}^{-1}$  or higher could be achieved in nanostructured arrays using just evaporation.

## Acknowledgments

We thank Professor Ping Sheng of HKUST for many useful comments and the referees for very constructive comments. This work was supported by grants from DARPA/ONR

(W911NF-05-1-0392, N00014-04-1-0776 and MDA972-00-1-0031), NSF Nanobiology Technology Center (BSCECS9876771) and the state of New Jersey (NJCST 99-100-082-2042-007).

## References

- [1] Huang L R, Cox E C, Austin R H and Sturm J 2004 Continuous C particle separation through deterministic lateral displacement *Science* **304** 987–90
- [2] Barthlott W and Neinhuis C 1997 Purity of the sacred lotus, or escape from contamination in biological surfaces *Planta* **202** 1–8
- [3] Oppenheim I and van Kampen N G 1983 The kinetic origin of the stick boundary condition *Physica A* **122** 277–85
- [4] Matthews M T and Hill J M 2008 Nanofluidics and the Navier boundary condition *Int. J. Nanotechnol.* **5** 218–42
- [5] Bocquet L and Barrat J L 2007 Flow boundary conditions from nano- to micro-scales *Soft Matter* **3** 685–93
- [6] Cottin-Bizonne C, Barrat J L, Bocquet L and Charlaix E 2003 Low-friction E flows of liquid at nanopatterned interfaces *Nat. Mater.* **2** 237–40
- [7] Lide D R (ed) 2005 *CRC Handbook of Chemistry and Physics, Internet Version 2005* (Boca Raton, FL: CRC Press) <http://www.hbcnpnetbase.com>
- [8] Purcell E M 1977 Life at low Reynolds number *Am. J. Phys.* **45** 3–11
- [9] De Gennes P G 1985 Wetting—statics and dynamics *Rev. Mod. Phys.* **57** 827–63
- [10] Bonn D, Eggers J, Indekeu J, Meunier J and Rolley E 2009 Wetting and spreading *Rev. Mod. Phys.* **81** 739–805
- [11] de Coninck J and Dunlop F 1987 Partial to complete wetting—a microscopic derivation of the Young relation *J. Stat. Phys.* **47** 827–49
- [12] Ausserre D, Picard A M and Leger L 1986 Existence and role of the precursor film in the spreading of polymer liquids *Phys. Rev. Lett.* **57** 2671–4
- [13] Wenzel R N 1949 Surface roughness and contact angle *J. Phys. Colloid Chem.* **53** 1466–7
- [14] McHale G, Shirtcliffe N J, Aqil S, Perry C C and Newton M I 2004 Topography driven spreading *Phys. Rev. Lett.* **93** 036102
- [15] Ishino C and Okumura K 2008 Wetting transitions on textured hydrophilic surfaces *Eur. Phys. J. E* **25** 415–24
- [16] Ishino C, Reyssat M, Reyssat E, Okumura K and Quere D 2007 Wicking within forests of micropillars *EPL* **79** 56005
- [17] Leger L, Erman M, Guinetpicard A M, Ausserre D and Strazielle C 1988 Precursor film profiles of spreading liquid drops *Phys. Rev. Lett.* **60** 2390–3
- [18] Courbin L, Denieul E, Dressaire E, Roper M, Ajdari A and Stone H A 2007 Imbibition by polygonal spreading on microdecorated surfaces *Nat. Mater.* **6** 661–4
- [19] Yu Z N, Chen L, Wu W, Ge H X and Chou S Y 2003 Fabrication of nanoscale gratings with reduced line edge roughness using nanoimprint lithography *J. Vac. Sci. Technol. B* **21** 2089–92
- [20] Murphy P F, Morton K J, Fu Z L and Chou S Y 2007 Nanoimprint mold fabrication and replication by room-temperature conformal chemical vapor deposition *Appl. Phys. Lett.* **90** 203115
- [21] Morton K J, Nieberg G, Bai S F and Chou S Y 2008 Wafer-scale patterning of sub-40 nm diameter and high aspect ratio silicon pillar arrays by nanoimprint and etching *Nanotechnology* **19** 345301